The electronic structure of simple models of amorphous solids: dangling bonds, hybridization and binary alloys

1994 J. Phys.: Condens. Matter 6 2215

(http://iopscience.iop.org/0953-8984/6/11/010)

J. Phys.: Condens. Matter 6 (1994) 2215–2224. Printed in the UK

The electronic structure of simple models of amorphous solids: dangling bonds, hybridization and binary alloys

Th Koslowski† and W von Niessen

Institut für Physikalische und Theoretische Chemie der TU, Hans-Sommer-Straße 10, D-38106 Braunschweig, Germany

Received 14 January 1994

Abstract. We report a numerical study of the electronic structure of a simple model for amorphous solids. The geometry of the model is described by continuous random networks based on the honeycomb lattice; the electronic structure is computed from simple tight-binding Hamiltonians. The density of states and the localization properties of eigenstates have been computed for an ideal random network and systems containing dangling bonds. Models including hybridization and alloy effects have been studied, both leading to the formation of impurity bands. The origin and the physical implications of these impurity bands are discussed.

1. Introduction

Continuous random networks (CRNs) are a model widely used to describe the geometry of both elementary and multicomponent amorphous solids with a strong covalent character of the chemical bond. In a CRN, each element retains its coordination number Z defined by the $8N$ rule. Deviations from the bond lengths and bond angles observed in the corresponding crystalline compounds are usually small, whereas no long-range topological order can be found. The CRN concept was introduced by Zachariasen [1], the first random network fulfilling the conditions described above was constructed by Polk to describe the geometry of amorphous silicon [2]. Recent work on CRNs covers the construction and relaxation of accurate models for a:Si and the computation of the electronic structure based on tight-binding Hamiltonians [3]. Systems with approximately 10^5 atoms have been generated and studied by the equation-of-motion method to compute the density of states and the electric conductivity [4].

As the translational invariance of crystalline compounds is destroyed in their amorphous counterparts, the eigenstates cannot be described in terms of Bloch functions. If the disorder present in a disordered system is strong enough, localization of all eigenstates due to disorder will occur [5]. For systems with a small degree of disorder such as CRNs, the density of states can be subdivided into regions containing localized states and regions dominated by extended states, separated by mobility edges [6]. The question of electron localization in models of amorphous solids has been addressed by Nichols and Winer [7] for a:Si. The present authors have studied electron localization for various Hamiltonians in two dimensions [8, 9] and for the distorted diamond lattice with Hamiltonians appropriate for a:Si, a:Ge and the hypothetical a:C [9, 10].

† Present address: Physical Chemistry Laboratory, University of Oxford, South Parks Road, Oxford OX1 3QZ, UK.

0953-8984/94/112215+10$19.50

In this article we study simple models of amorphous solids to investigate the influence of dangling bonds, hybridization and alloy effects. We expect the effects observed for these highly simplified models to be of general relevance to amorphous systems, regardless of the dimension. Any detailed comparison to experimental data is out reach for systems as highly simplified as those presented here, although a parametrization corresponding to boron nitride has been used for the binary alloy. None of the properties computed is unique to two-dimensional systems; however, the generation of dangling bonds is much simpler for the hexagonal than for the diamond lattice. In this article we present the construction of a model system in two dimensions, based on the honeycomb lattice, that allows the description of both ideal CRNs free of defects and of CRNs containing dangling bonds as one of the most important types of defect present in amorphous solids. The electronic structure will be described by a simple tight-binding Hamiltonian with one basis function centred on each atom, later to be extended to include hybridization effects and to allow for the description of multicomponent systems, in this article a simple binary alloy. The article is organized as follows. In the next section, we present the method used to construct CRNs and the procedures to compute the density of states and the localization properties of the system. As four different types of model have been studied, the details of each model, including the Hamiltonian, the results obtained and a brief discussion will be presented in four distinct subsequent sections. Conclusions are derived in the last section.

2. Methods

Whereas the first CRNs had been built by hand [2], the construction of CRNs utilizing a computer was quickly recognized as a powerful tool to study the geometry of models of amorphous systems [11]. In this work, we use a simple vacancy model similar to the work of Duffy *et al* [11]. We have refrained from implementing one of the more sophisticated algorithms appropriate for the study of a:Si ([3], [4], to mention a few) because the main purpose of the models presented in this work is not the accurate simulation of an existing compound, but the description of basic phenomena by highly simplified models.

To construct a CRN on the honeycomb lattice, the following procedure is repeated until a given concentration p of defects has been created: choose an atom at random; eliminate this atom and one of its three neighbours, again chosen at random. The double vacancy constructed this way is surrounded by four dangling bonds. From these four danging bonds, two covalent bonds are created in such a way that a structure that used to contain four six-membered rings centred around the double vacancy is now replaced by two five-membered rings and one eight-membered ring. The creation of rings with less than five members is not allowed. Care has been taken not to create double bonds, small rings or large clusters of vacancies. In practice, these restrictions allow the construction of CRNs with a concentration of defects up to 0.1. The concentration p of double vacancies serves as the disorder parameter of the system. Cyclic boundary conditions have been imposed. A CRN created by the algorithm described above is presented in figure 1(a).

In a similar way, a random network containing dangling bonds as defects can be constructed. Again, an atom is chosen at randon and eliminated, leaving three dangling bonds around a single vacancy. Out of these three bonds, two are reconnected at random, leaving one dangling bond. So three six-membered rings around a vacancy have been replaced by a five-membered and a nine-membered ring. A lattice resulting from this procedure is shown in figure 1(b). Both types of random network contain odd-membered rings, which have a crucial effect on the electronic structure [12]: the lattice is not bipartite

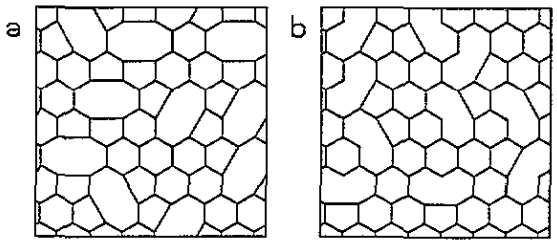

Figure 1. CRNs constructed from the honeycomb lattice: (a) an ideal random network; (b) a system containing dangling bonds.

like the ideal honeycomb lattice; the density of states is asymmetric, i.e. at half-filling the particle-hole symmetry has been broken. As the sign of eigenstates close to the upper band edge cannot vary from site to site any longer, this phenomenon is called frustration in analogy to spin systems with the same topology. Random networks based on the hexagonal lattice may also be created using bond flipping [13] or dislocation processes [14].

For all models, a simple tight-binding Hamiltonian

$$H = \sum_{ia} \epsilon_{ia} c_{ia}^{\dagger} c_{ia} + \sum_{i \neq j, a, b} V_{iajb} c_{ia}^{\dagger} c_{jb} \tag{1}$$

is used to describe the electronic structure on top of the CRN. The operators $c_{ia}^{\dagger}$ and c_{ia} create and annihilate atomic orbitals localized at site i. To make a distinction between different basis functions localized at the same site, the additional index a has been introduced. ϵ_{ia} is the site energy of orbital $|ia\rangle$, the hopping matrix element V_{iajb} is non-zero for nearest neighbours only. To solve the large sparse eigenvalue problems originating from this tight-binding Hamiltonian, a Lanczos algorithm has been used [15].

To decide about the localized or extended nature of eigenstates, we use the small-decoupling version [8] of the method of Thouless, Edwards and Licciardello [16], abbreviated to TEL, in connection with a scaling principle. As details of the method used can be found in [8] and [10], we will only give a brief outline here. TEL were able to show that the energy shift ΔE caused by a change in boundary conditions is related to the conductance g by

$$g(L, p, E) \propto \frac{\Delta E(L, p, E)}{\delta E(L, p, E)} \tag{2}$$

where L denotes the system length, δE the average level spacing and p the disorder parameter. Following the scaling theory of localization [17], the eigenstates within an energy interval for a given degree of disorder are identified as being localized if $g(L)$ decreases with increasing L, whereas if $g(L)$ increases with increasing L, the eigenfunctions are extended. ΔE and δE are usually taken as geometric averages within a certain energy interval. The TEL method will be illustrated in section 6 for the most complicated pattern of mobility edges studied in this work, enabling a judgment about the quality of the determination of localization properties.

3. The ideal random network

As a reference system, we have studied the ideal CRN without any dangling bonds. A set of orbitals centred at the sites of the CRN is used as the basis set, the interaction has been

set to a constant for nearest neighbours, with $V_{iajb} = V_{ij} = V = -\frac{1}{3}$. All ϵ_i have been set to zero, so the disorder is of topological nature only. Systems exhibiting the vacancy concentrations $p = 0.02$, $p = 0.04$ and $p = 0.08$ have been studied for models containing 1008 ($R = 120$), 1792 ($R = 39$), 2800 ($R = 16$) and 4032 ($R = 6$) atoms, where R denotes the minimum number of realizations performed for each system size. For the last two concentrations, additional calculations have been performed for systems containing 5376 atoms in the ideal random network ($R = 5$).

The density of states (DOS) is presented in figure 2; energy intervals containing localized wavefunctions according to the TEL analysis have been shaded. The DOS is asymmetric even at a vacancy concentration as low as $p = 0.02$, but there is no evidence for localized eigenstates in any of the energy intervals. Remainders of the logarithmic singularities of the crystalline honeycomb lattice can be observed at $E = \pm\frac{1}{3}$. With increasing vacancy concentration, localized states are formed at the upper band edge, accompanied by a decreasing DOS. An interesting phenomenon can be observed at $p = 0.04$: the formation of an interval of localized states at the Fermi level, favoured by the small density of states at E_F. At $p = 0.02$, the amount of disorder is too small to create localized states, whereas at $p = 0.08$ the DOS is large enough to suppress localization despite the increasing degree of disorder, a phenomenon also observed in models of a:Si [10]. It should be noted that for all values of p studied the conductance values at E_F are very small and comparable to that at the band edge, so Fermi-level localization cannot be ruled out completely for p values different from $p = 0.04$.

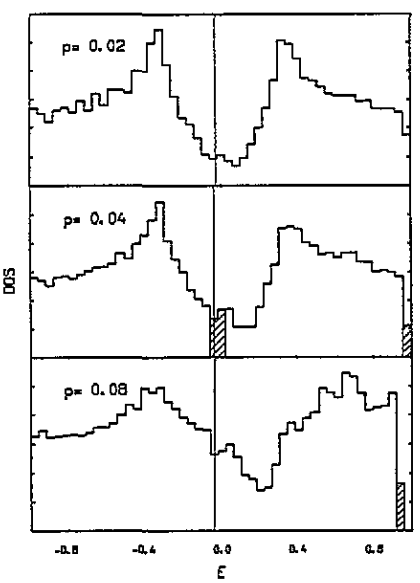

Figure 2. The DOS of the ideal random network for three different vacancy concentrations p. Energy is in units of 1/Z; DOS is in arbitrary units. Localized regions have been shaded; the solid line indicates the Fermi level.

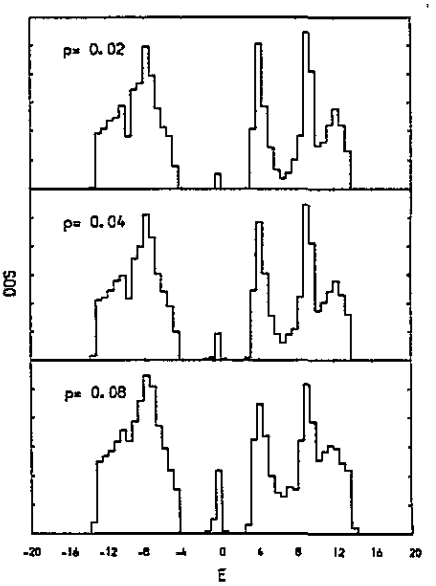

Figure 3. The DOS of the hybridization model for three different vacancy concentrations p. Energy is in electronvolts; DOS is in arbitrary units.

A discussion of the localization properties of eigenstates in two dimensions cannot be complete without reference to the scaling theory of localization [17], which predicts the

localization of all eigenstates in two dimensions. Supported by numerical calculations for the Anderson model [18], there are considerable doubts whether the scaling theory holds for systems with topological disorder such as the quantum percolation problem [20, 21, 19]; for a brief review on quantum percolation and the opposite point of view see [22]. For CRNs with a constant number Z of nearest neighbours and uniform $\epsilon_i = 0$ there is a simple proof that at least one extended eigenstate exists regardless of the Euclidian dimension. Writing down the eigenvalue equation (1) for an arbitrary row i of the Hamiltonian matrix

$$-E_\alpha a_{i\alpha} - V \sum_{j=1}^{Z} a_{j\alpha} = 0 \tag{3}$$

it is obvious that (3) is fulfilled by $E = -ZV$ and $a = (a_1, a_2, a_3, \ldots) = (1, 1, 1, \ldots)$ for all i. According to the the theorem of Hadamard and Gershgorin, $-ZV$ is a lower bound to the spectrum of H, so the existence of an extended eigenstate at the lower band edge can be proved. It is interesting to note that the lower band edge does not erode with increasing p, so the features of the lowest eigenstate are unlikely to be singular.

4. Dangling bonds

The dangling-bond CRN has been studied for vacancy concentrations of $p = 0.02$, $p = 0.04$ and $p = 0.08$. To perform the TEL analysis, the dimensionless conductance has been computed for systems containing 1008 ($R = 83$), 1792 ($R = 28$), 2800 ($R = 12$) and 4032 ($R = 6$) atoms. In addition, for $p = 0.04$, a 5376-atom system has been studied ($R = 5$). We have used the Hamiltonian described in the preceding sections. The DOS is very similar to the DOS of the ideal CRN, so it is not plotted here. The major difference can be observed at the lower band edge, which now erodes with increasing p. As Z is not constant for this type of network, this behaviour is not surprising. Equation (3) is no longer fulfilled by the solution given above. Localized states can be observed at the upper band edge for $p = 0.04$ and $p = 0.08$, covering about the same region of the spectrum as for the ideal CRN. No localized states can be detected at the lower band edge. So in contrast to the introduction of a distance-dependent V [8], the creation of dangling bonds is not sufficient to induce localization. No localized states can be detected around the Fermi level. Again, the g value computed at E_F for larger vacancy concentrations has the same order of magnitude as the g value found at the upper band edge, so localization cannot be ruled out in the middle of the band.

5. Hybridization

To study hybridization effects, we used a basis set of s and p orbitals on each atom. The ϵ_{is} parameter, defining the site energy of the s orbital at site i, has been set to zero; the ϵ_{ip} parameter has been set to 7.20 eV. The energy difference is the same as used for the tight-binding description of Si [23]. The V_{iajb} hopping matrix elements are computed from the Slater–Koster [24] formulae, the following parameters have been chosen: $V_{ss\sigma} = -2.71$ eV, $V_{sp\sigma} = 3.40$ eV, $V_{pp\sigma} = 6.07$ eV and $V_{pp\pi} = -1.45$ eV. All hopping-matrix elements are independent of the interatomic distance. They are equal to $\frac{4}{3}$ of the Harrison parameters for Si taking into account the reduction of the coordination number from four (diamond lattice) to three (hexagonal lattice). The CRN has not been relaxed, so an additional off-diagonal

disorder has been introduced, which results from the non-uniformity of the bond-angle distribution.

Again, the density of states and localization properties have been computed for $p = 0.02$, $p = 0.04$ and $p = 0.08$. The following system sizes have been studied: 336 atoms ($R = 87$), 448 atoms ($R = 49$), 576 atoms ($R = 29$) and 680 atoms ($R = 21$). The results can be observed for the CRN containing dangling bonds. The DOS is plotted in figure 3. The valence band exhibits a shallow minimum at -10 eV, disappearing with increasing vacancy concentration. A similar phenomenon can be observed in the conduction band. The highly structured density of states that can be observed for $p = 0.02$ erodes with increasing p. Around $E = 0$, in the former band gap, an impurity band is formed. Both the integrated DOS and the width of the impurity band increase with increasing vacancy concentration. The impurity band consists predominantly of states localized on atoms whose bonds are unsaturated. The eigenfunctions are not localized on a single atom only, but cover several defects that are close neighbours. At half filling, the Fermi level lies in the middle of the impurity band, so the transport properties of the system will be dominated by defects. A TEL analysis has been performed for the impurity band, showing that all eigenstates within the band are localized up to $p = 0.08$. As the impurity band is rather narrow, it is likely to exhibit a gap or a pseudogap once electron–electron interaction is introduced [25].

We think that the properties observed for the model described in this chapter are universal for amorphous systems with dangling bonds and a band gap in the crystalline phase. Although the number of dangling bonds in any realistic model of a:Si is one to two orders of magnitude smaller, the domination of the transport properties by defects and the potential sensitivity to electron–electron interaction effects should also be observed there.

6. Binary systems

The simplest type of multicomponent system is the binary alloy AB. The Hamiltonian described in section 3 has been modified by the introduction of a site energy $\epsilon_B \neq 0$ for one type of atom. The ϵ_A parameter defines the zero of the energy scale; the ϵ_B parameter has been set to $5V$. For a binary alloy, the specification of the geometry not only requires knowledge of the topology of the system, but also the distribution of A and B atoms on the sites of the system. Starting from a crystalline honeycomb lattice with each A atom surrounded by three B atoms as nearest neighbours and vice versa (this is, e.g., the structure of BN), we generate the ideal CRN described in section 2 by removing A and B atoms that are nearest neighbours with equal probability p. Obviously, this procedure creates A–A and B–B bonds, defects that are not present in the crystalline phase. We were particularly interested in the influence of these bond mismatch defects on the electronic structure.

The DOS and the localization properties of the AB alloy have been computed from CRNs generated from lattices containing 1008 atoms ($R = 118$), 1792 atoms ($R = 38$), 2800 atoms ($R = 16$) and 4032 atoms ($R = 7$). Figure 4 illustrates the TEL analysis performed for this system. The scaling behaviour of the negative logarithm of the dimensionless conductance g is plotted as a function of energy. The energy interval $(-1, \frac{3}{2})$ has been subdivided into 48 bins. Within each bin the average of $-\ln g$ is plotted as a function of the system size L, L increasing from left to right. Whenever g increases with increasing system size, i.e. $-\ln g$ decreases with increasing L, the corresponding eigenstates are extended. In the opposite case, the wavefunctions show a localized character and the interval is labelled accordingly. For $p = 0.02$, localized states can be found at the top of the valence band and at the bottom of the conduction band. The alternation of localized and extended states observed for $p = 0.04$ and $p = 0.08$ will be resolved as soon as the DOS is studied.

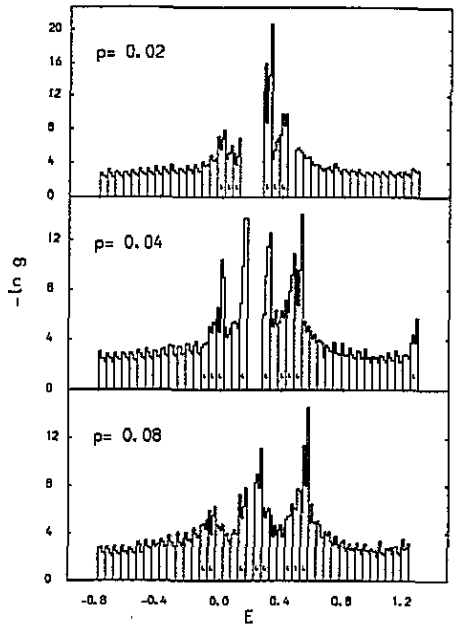

Figure 4. TEL analysis of the alloy model for three different vacancy concentrations p: the negative logarithm of the dimensionless conductance as a function of energy. Energy is in units of $1/Z$. Localized intervals have been marked by an L. For details see the text.

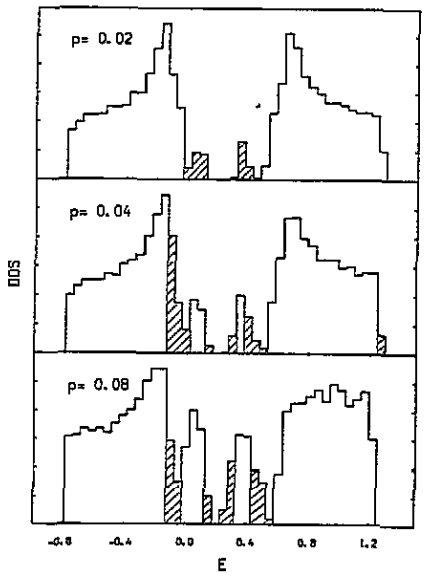

Figure 5. The DOS of the alloy model for three different vacancy concentrations p. Energy is in units of $1/Z$; DOS is in arbitrary units. Localized regions have been shaded.

The DOS for the vacancy concentrations listed above is presented in figure 5. For all vacancy concentrations, two impurity bands split from the top of the valence band and the bottom of the conduction band. The separation of the impurity bands from the bulk of the DOS is more evident for the valence band. As usual, regions containing localized states according to the TEL analysis have been shaded. At $p = 0.02$, all states within the impurity bands are localized. At $p = 0.04$, a transition from localized to extended states within the impurity bands can be observed where the impurity band DOS shows a local maximum. The regions connecting the impurity bands to the bulk of the DOS and the band edges close to the band gap still exhibit a localized behaviour. At $p = 0.08$, both the integrated DOS and the number of extended states within the impurity bands have considerably increased. The interval containing extended states within the impurity band is wider at the top of the valence band than at the bottom of the conduction band.

What is the reason for the formation of these impurity bands and the transition from localized to extended states in these bands? To answer these questions, we have performed a population analysis [26]. With the charge order at site i and for an eigenstate $|\alpha\rangle$ of the Hamiltonian given by

$$q_i^\alpha = \langle\alpha|i\rangle\langle i|\alpha\rangle = a_{i\alpha}^2 \tag{4}$$

we can define the charge order corresponding to a set of sites by taking the sum of all q_i^α for all i of the corresponding set of sites. We have computed the charge order for the following types of site: q_{AB} for A atoms connected to three B atoms, q_{BA} for B atoms connected to three A atoms, q_{AA} for an A atom connected to one A atom and two B atoms

and q_{BB} for a B atom connected to one B atom and two A atoms. The latter two charge orders refer to wrong bonds as described above. We have taken averages of these quantities. The charge order dominating in each interval is indicated in figure 6 for the three vacancy concentrations studied for this model. Each type of q is indicated by a different symbol. The bulk of the valence band is dominated by q_{AB} states, the bulk of the conduction band by q_{BA} states. The impurity band at the top of the valence band is dominated by q_{AA}, and the one at the bottom of the conduction band by q_{BB}; q_{AA} has a maximum at the top of the valence band, q_{BB} a maximum at the bottom of the conduction band. Although the total number of wrong bonds is small, they dominate the impurity bands. There is a sharp jump in the character of eigenstates at the local minima of the DOS between the bulk of the spectrum and the impurity bands. With increasing p, the number of wrong bonds increases; these can couple and form extended states.

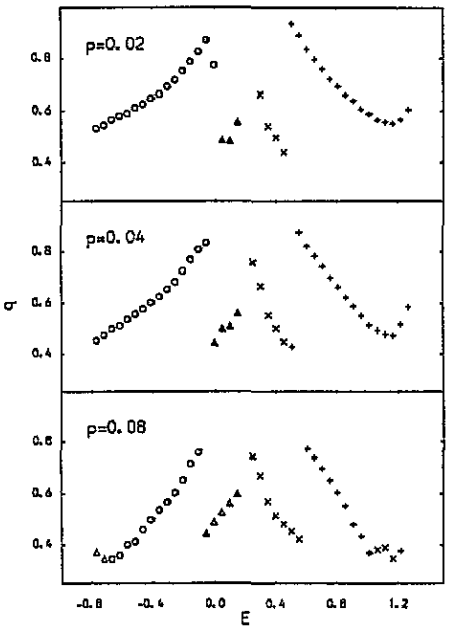

Figure 6. A population analysis for the alloy model for three different vacancy concentrations p. Energy is in units of 1/Z; charge orders, q_{AB} (○), q_{AA} (△), q_{BB} (×) and q_{BA} (+).

The binary-alloy model does not only describe multicomponent systems (actually, the tight-binding parameters are appropriate for the two-dimensional layer compound BN) but has an interesting connection to interacting systems. Introducing on-site repulsion between electrons of different spin for the Hamiltonian described in section 3, the familiar Hubbard Hamiltonian [25, 27, 28] is obtained:

$$H = V \sum_{ij\sigma} c_{i\sigma}^{\dagger} c_{j\sigma} + \frac{U}{2} \sum_{i\sigma} n_{i\sigma} n_{i-\sigma}. \tag{5}$$

U measures the strength of the electron–electron interaction, σ is the spin index and $n_{i\sigma}$ the number operator for a σ-spin electron at site i. In the unrestricted Hartree–Fock (UHF) approximation equation (5) can be written as

$$H_{\sigma} = V \sum_{ij} c_{i\sigma}^{\dagger} c_{j\sigma} + U \sum_{i} n_{i\sigma} \langle n_{i-\sigma} \rangle \tag{6}$$

and a similar equation for electrons with spin $-\sigma$. If the expectation value $\langle n_{i-\sigma} \rangle$ is known, equation (6) reduces to a one-electron problem. The solution of the one-electron problem by a procedure similar to the coherent-potential approximation is known as the Hubbard III approximation [28]. Identifying $U\langle n_{i-\sigma} \rangle$ with ϵ_B recovers the binary alloy. In the large-U limit at half filling, the Hubbard Hamiltonian can be transformed into the Heisenberg model [29]. On a bipartite lattice at zero temperature, antiferromagnetism will be observed, corresponding to a bipartite decoration with A and B atoms. For a frustrated antiferromagnet (amorphous binary alloy), the ordering of the eigenstates of the mean-field (or binary-alloy) Hamiltonian can be easily understood: the lowest occupied eigenstates can be described as σ-spin electrons (A atoms) surrounded by three $-\sigma$-spin electrons (B atoms), giving rise to a maximum antiferromagnetic coupling. These are followed by σ-spin electrons (A atoms) with a single wrong bond, giving rise to a local ferromagnetic repulsion and thus a higher energy. The same argument holds for the unoccupied eigenstates of the Hamiltonian (6). So the analogy—which is by no means an identity—of the binary-alloy model and the Hubbard model in the large-U limit helps us to understand the ordering of the energies and the origin of the impurity bands. It should be noted that the energies of the eigenstates of the Hamiltonian (6) do not describe the low-energy part of the spectrum of single-particle (and hole) excitations of the Hubbard model for the given choice of parameters accurately, because the formation of spin waves requires an energy much smaller than the band gap.

7. Conclusions

We have studied CRNs in two dimensions as a simple model for amorphous solids. The electronic properties—with a special emphasis on the localized or extended character of eigenstates—have been computed for a variety of tight-binding Hamiltonians. The ideal lattice with a single s- or p_z-like orbital on each site shows localization or a very small conductance at the top of the band and in addition at the Fermi level for a certain combination of parameters, similar to the results that Varga and Pipek [30] have presented for a two-dimensional model of a:C [31]. The existence of at least one extended state for ideal CRNs in two dimensions has been proved rigorously. For s-like orbitals, the introduction of dangling bonds does not change the electronic structure significantly.

Hybridization effects in a Hamiltonian that describes a CRN containing dangling bonds lead to the formation of a narrow impurity band in the middle of the gap that determines the transport properties of the system. The DOS and the localization properties of the impurity band are likely to be sensitive to electron–electron interaction effects.

As a simple model for a multicomponent system, a binary alloy model—corresponding to the BN layer compound—has been studied. Impurity bands split off from both the valence band and the conduction band. The corresponding states are localized in the regime of small defect concentrations. With increasing p the integrated DOS in the impurity bands increases, and a transition from a localized to an extended character of the eigenstates at the centre of the impurity bands is observed. This is a replay of the situation found in one-band models of Anderson localization. A population analysis reveals the binding situation. The bulk valence band is dominated by states where the A atoms are surrounded by three B atoms, the conduction band by states where the B atoms are surrounded by three A atoms. The valence impurity band is dominated by states where the A atoms see one wrong bond (pointing to another A atom), and the conduction impurity band by states where the B atoms see one wrong bond.

The Hubbard Hamiltonian can in the UHF approximation—with further simplifications—be reduced to the binary-alloy Hamiltonian. In the large-U (Heisenberg-model) limit, an anology of the amorphous AB model with a frustrated antiferromagnet has been presented.

Acknowledgments

It is a pleasure to thank B Kramer (PTB Braunschweig), D E Logan (Oxford), J Pipek (TU Budapest), L Schweitzer (PTB Braunschweig) and P Thomas (Marburg) for fruitful discussions. Financial support of the Deutsche Forschungsgemeinschaft and partial support of the Fonds der Chemischen Industrie is gratefully acknowledged. The computations were performed on the IBM 3090/600 VF vector computer of the computing centre of the TU Braunschweig.

References

[1] Zachariasen W H 1932 *J. Am. Chem. Soc.* **54** 3841
[2] Polk D E 1971 *J. Non-Cryst. Solids* **5** 365
[3] Wooten F, Winer K and Weaire D 1985 *Phys. Rev. Lett.* **54** 1395
[4] Holender J M and Morgan G J 1991 *J. Phys.: Condens. Matter* **3** 7241; 1992 *J. Phys.: Condens. Matter* **4** 4473
[5] Anderson P W 1958 *Phys. Rev.* **109** 1492
[6] Banyai L 1964 *Physique de Semiconducteurs* ed M Hulin (Paris: Dunod) p 417
[7] Nichols C S and Winer K 1988 *Phys. Rev.* B **38** 9850
[8] Koslowski Th and von Niessen W 1992 *J. Phys.: Condens. Matter* **4** 1093
[9] Koslowski Th and von Niessen W 1992 *Ber. Bunsenges. Phys. Chem.* **96** 1599
[10] Koslowski Th and von Niessen W 1992 *J. Phys.: Condens. Matter* **4** 6109
[11] Duffy M G, Boudreaux D S and Polk D E 1974 *J. Non-Cryst. Solids* **15** 435
[12] Singh J 1981 *Phys. Rev.* B **23** 4156
[13] Rivier N and Weaire D 1984 *J. Contemp. Phys.* **25** 59
[14] Robertson J 1992 *Phil. Mag.* B **66** 199
[15] Lanczos C 1950 *J. Res. NBS* B **45** 225
Cullum J K and Willoughby R K 1985 *Lanczos Algorithms for Large Symmetric Eigenvalue Problems* vols I and (Boston, MA: Birkhäuser)
Koslowski Th and von Niessen W 1993 *J. Comput. Chem.* **14** 769
[16] Edwards J T and Thouless D J 1972 *J. Phys. C: Solid State Phys.* **5** 807
Licciardello D C and Thouless D J 1975 *J. Phys. C: Solid State Phys.* **8** 4157; 1978 *J. Phys. C: Solid State Phys.* **11** 925
[17] Abrahams E, Anderson P W, Licciardello D C and Ramakrishnan T V 1979 *Phys. Rev. Lett.* **42** 673
[18] MacKinnon A and Kramer B 1983 *Z. Phys.* B **53** 1
[19] Srivastava V and Chaturvedi M 1984 *Phys. Rev.* B **30** 2238
[20] Meir Y, Aharony A and Harris A B 1989 *Europhys. Lett.* **10** 275
[21] Koslowski Th and von Niessen W 1990 *Phys. Rev.* B **42** 10342
[22] Mookerje A, Chakrabarti B K, Dasgupta I and Saha T 1992 *Physica* A **186** 258
[23] Harrison W A 1980 *Electronic Structure and the Properties of Solids* (San Francisco: Freeman)
[24] Slater J C and Koster G F 1954 *Phys. Rev.* **94** 1498
[25] Mott N F 1956 *Can. J. Phys.* **34** 1356; 1961 *Phil. Mag.* **6** 287
[26] Hoffman R 1963 *J. Chem. Phys.* **39** 1397
[27] Hubbard J 1963 *Proc. R. Soc.* A **276** 238
[28] Hubbard J 1964 *Proc. R. Soc.* A **281** 401
[29] Chao K A, Spalek J and Oles J 1977 *J. Phys.: Condens. Matter* **10** L271
Gros C, Joynt R and Rice T M 1988 *Phys. Rev.* B **37** 3759
[30] Varga I and Pipek J 1990 *Phys. Rev.* B **42** 5335
[31] Beeman D, Silverman J, Lynds R and Anderson M R *Phys. Rev.* B **30** 870